A&A 514, A40 (2010)
DOI: 10.1051/0004-6361/200913006

Astronomy & Astrophysics

Atomic data from the IRON project

LXVIII. Electron impact excitation of Fe XI*

G. Del Zanna[1], P. J. Storey[2], and H. E. Mason[1]

[1] DAMTP, Centre for Mathematical Sciences, Wilberforce Road Cambridge, CB3 0WA, UK
e-mail: G.Del-Zanna@damtp.cam.ac.uk
[2] Department of Physics and Astronomy, University College London, Gower Street, London, WC1E 6BT, UK

Received 28 July 2009 / Accepted 11 January 2010

ABSTRACT

A new R-matrix scattering calculation for electron collisional excitation of Fe XI is presented and compared to earlier calculations. The calculation includes 145 *LS* terms and 465 fine-structure levels and uses the intermediate-coupling frame transformation method (ICFT). We discuss the strong interactions that exist between three $J = 1$ levels in the $3s^2\ 3p^3\ 3d$ electron configuration. These levels give rise to strong lines in the EUV spectrum and their energies and identifications have been the source of much confusion in the literature. We show that the oscillator and collision strengths linking these levels to the ground levels of the ion are very sensitive to the choice of configuration basis and argue that most earlier calculations have failed to represent these levels adequately.

Key words. atomic data – line: identification – techniques: spectroscopic

1. Introduction

Fe XI is an important ion for the quiet solar corona because it produces strong spectral lines that can be used both for plasma diagnostics and for instrument calibration. Spectral lines from Fe XI have been recorded by many solar coronal missions (e.g. Skylab, SOHO), and are of particular importance for the recent Hinode mission, in particular the Extreme ultraviolet Imaging Spectrometer (EIS), as discussed e.g. in Young et al. (2007).

To date, there have been many scattering calculations for electron collisional excitation of Fe XI, all of which are unsatisfactory in some regard when comparisons are made with observations.

The first extensive work on this ion was from Mason (1975), who performed a distorted-wave (DW) calculation using the University College London (UCL) suite of codes. This work enabled Mason & Nussbaumer (1977) to confirm line identifications in the EUV.

Bhatia & Doschek (1996, hereafter BD96) performed a DW calculation using the same codes, and a basic set of 4 electron configurations ($3s^2\ 3p^4$, $3s\ 3p^5$, $3s^2\ 3p^3\ 3d$, $3p^6$) for their scattering calculation. These calculations were then extended by Bhatia et al. (2002, hereafter BDE02) by including some $n = 4$ levels, for a total of 96 fine-structure levels.

Gupta & Tayal (1999a,b, hereafter GT99) calculated collision strengths for transitions between 38 fine-structure levels using a semi-relativistic R-matrix approach. Large differences with the DW results of Bhatia & Doschek (1996) were found, partly due to the resonance contribution, partly due to the use of a different target and configuration basis. GT99 adopted a 20 *LS* state target, expanded in a 78-state basis, from Deb & Tayal (1998, hereafter DT98). We note that this 20 state calculation is not actually described in Deb & Tayal (1998) but as discussed below, is not in good agreement with the experimental data. Moreover, the GT99 calculation was incomplete from an application point of view, because it did not include the important ^{5}D, ^{3}G^o and ^{1}G^o *LS* terms. Some of the levels originating from these terms are metastable and it is necessary to include them when calculating the level populations. Aggarwal & Keenan (2003a,b, hereafter AK03) used an 8-configuration basis for their scattering calculation, in which they included configuration-interaction (CI) among the four main spectroscopic configurations and the additional $3s^2\ 3p^2\ 3d^2$, $3s^2\ 3p^3\ 4s$, $3s^2\ 3p^3\ 4p$, and $3s^2\ 3p^3\ 4d$ configurations. There are various problems with the above calculations, mostly due to the strong interactions present between some Fe XI levels, as described below.

2. The target and the line identifications

The construction of a good target has been particularly challenging for this ion. This is because the energies of a large number of fine-structure levels have remained unknown experimentally, and there is strong level mixing among some levels, in particular for the three energetically highest $J = 1$ levels in the $3s^2\ 3p^3\ 3d$ configuration. These levels are important because they give rise to some of the strongest Fe XI spectral lines, which fall in the EUV.

As part of the preliminary work to identify the best target we re-assessed all the literature and experimental data not only for Fe XI, but also for many of the ions along the same S I-like isoelectronic sequence. Most previous line identifications have been made using laboratory measurements. For the Fe ions in particular see the work by Fawcett and the group at the Culham laboratories in the 1960's and 70's (see, e.g. Fawcett & Gabriel 1965; Gabriel et al. 1965; Fawcett & Gabriel 1966; Gabriel et al. 1966; Bromage et al. 1977). Further work has been

* Detailed tables of the present data are available in electronic form at the CDS via anonymous ftp to cdsarc.u-strasbg.fr (130.79.128.5) or via http://cdsweb.u-strasbg.fr/cgi-bin/qcat?J/A+A/514/A40

produced by a few other authors (e.g. Jupén et al. 1993; Träbert et al. 2003), however some level and line identifications were contradictory.

The spectra obtained at the Culham laboratories were not free from impurities, but had an excellent spectral resolution and are still the best available to identify lines that are formed in high-density plasmas. As part of the assessment we have re-analysed some of the original plates, and used some unpublished material from Fawcett. The spectral resolution was slightly better than the quiet-Sun integrated rocket spectrum of Behring et al. (1976) which has become the basic reference for many wavelength measurements. The result of this work, and in particular what we refer to here as our experimental energies $E_{\rm exp}$, will be published in a separate paper (Del Zanna 2010).

2.1. Previous structure calculations

The main (spectroscopically important) configurations for Fe XI are $3s^23p^4$, $3s\,3p^5$, $3s^23p^33d$, and $3p^6$, which give rise to 48 fine-structure levels. Decays from $3s\,3p^5$ and $3s^23p^33d$ to the ground configuration $3s^23p^4$ produce strong EUV lines. Additional lines in the X-ray are produced mostly by decays from $n = 4$ levels.

Bromage et al. (1977) used Cowan's Hartree-Fock (HF) atomic structure code with the Slater parameters optimization procedure to provide experimentally-adjusted energies for the $3s^2\ 3p^3\ 3d$ levels, and oscillator strengths for transitions from these levels to the ground configuration. This was an excellent piece of work, showing the importance of combining laboratory measurements with atomic structure calculations, something rarely found in the literature. Fawcett (1986) used the Hartree-Fock-Relativistic code of Cowan with the Slater parameters optimization procedure to provide $3s^2\ 3p^3\ 3d$ level energies and oscillator strengths for $3s^2\ 3p^4$–$3s^2\ 3p^3\ 3d$ transitions in various ions of the S I-like sequence. The adjustments took into account the experimental wavelengths available at that time, and only included CI among the main four configurations and the additional $3s\ 3p^4\ 3d$, $3p^5\ 3d$, $3s\ 3p^3\ 3d^2$ and $3s^2\ 3p^3\ 4s$ configurations.

Mendoza & Zeippen (1983) calculated transition probabilities for the forbidden transitions in the ground configuration along the isoelectronic sequence by using SUPERSTRUCTURE (see Eissner et al. 1974; Nussbaumer & Storey 1978) and a set of eight configurations.

BD96 used a basic set of four configurations within SUPERSTRUCTURE. These calculations were then extended by BDE02 by including some $n = 4$ levels, for a total of 96 fine-structure levels. We note that this extension did not significantly alter oscillator strengths for transitions to the $3s^2\ 3p^3\ 3d$ levels, i.e. did not improve the representation of the $n = 3$ configurations.

Fritzsche et al. (2000) calculated transition probabilities for forbidden and allowed Fe XI transitions using the GRASP92 atomic structure code and a multiconfiguration Dirac-Fock (MCDF) approach. Unfortunately, no adjustments to experimental energies were applied, nor experimental wavelengths used in the calculations of the transition probabilities. Large discrepancies (more than 50 Å) between their calculated wavelengths and the observed ones are present, particularly for the forbidden lines.

DT98 calculated ab initio energies and oscillator strengths with the CIV3 atomic structure code by initially including all configurations (up to $n = 4$) with 2-electron excitations from the basic four configurations.

Table 1. Electron configuration basis for the benchmark calculation (48C) and orbital scaling parameters.

Configurations		Scaling parameters[†]	
even	odd		
$3s^2\ 3p^4$	$3s\ 3p^5$	1s	1.41166
$3p^6$	$3s^2\ 3p^3\ 3d$	2s	1.12282
$3s\ 3p^4\ 3d$	$3p^5\ 3d$	2p	1.06334
$3s^2\ 3p^2\ 3d^2$	$3s\ 3p^3\ 3d^2$	3s	1.14302
$3p^4\ 3d^2$	$3s^2\ 3p\ 3d^3$	3p	1.09982
$3s\ 3p^2\ 3d^3$	$3p^3\ 3d^3$	3d	1.11949
$3s^2\ 3p^3\ \overline{4}p$	$3s^2\ 3p^3\ \overline{4}s$	$\overline{4}s$	–0.69087
$3s^2\ 3p^3\ \overline{4}f$	$3s^2\ 3p^3\ \overline{4}d$	$\overline{4}p$	–0.66353
$3s\ 3p^4\ \overline{4}s$	$3s\ 3p^4\ \overline{4}p$	$\overline{4}d$	–1.28354
$3s\ 3p^4\ \overline{4}d$	$3s\ 3p^4\ \overline{4}f$	$\overline{4}f$	–0.82606
$3p^5\ \overline{4}p$	$3p^5\ \overline{4}s$	$\overline{5}s$	–1.20021
$3p^5\ \overline{4}f$	$3p^5\ \overline{4}d$	$\overline{5}p$	–1.22563
$3s^2\ 3p^2\ 3d\ \overline{4}s$	$3s^2\ 3p^2\ 3d\ \overline{4}p$	$\overline{5}d$	–1.10475
$3s^2\ 3p^2\ 3d\ \overline{4}d$	$3s^2\ 3p^2\ 3d\ \overline{4}f$	$\overline{5}f$	–1.63546
$3s^2\ 3p^3\ \overline{5}p$	$3s^2\ 3p^3\ \overline{5}s$	$\overline{5}g$	–1.20870
$3s^2\ 3p^3\ \overline{5}f$	$3s^2\ 3p^3\ \overline{5}d$		
$3s\ 3p^4\ \overline{5}s$	$3s^2\ 3p^3\ \overline{5}g$		
$3s\ 3p^4\ \overline{5}d$	$3s\ 3p^4\ \overline{5}p$		
$3s\ 3p^4\ \overline{5}g$	$3s\ 3p^4\ \overline{5}f$		
$3p^5\ \overline{5}p$	$3p^5\ \overline{5}s$		
$3p^5\ \overline{5}f$	$3p^5\ \overline{5}d$		
$3s^2\ 3p^2\ 3d\ \overline{5}s$	$3p^5\ \overline{5}g$		
$3s^2\ 3p^2\ 3d\ \overline{5}d$	$3s^2\ 3p^2\ 3d\ \overline{5}p$		
$3s^2\ 3p^2\ 3d\ \overline{5}g$	$3s^2\ 3p^2\ 3d\ \overline{5}f$		

Notes. [†] See text for the physical significance of the scaling parameters.

2.2. Our target

We have carried out a large number of structure calculations with different sets of configurations and orbitals using SUPERSTRUCTURE and AUTOSTRUCTURE (Badnell 1997). We found that the positioning and mixing of some levels changes considerably, strongly affecting energies and oscillator strengths. We have also made structure calculations using the same set of configurations as those reported in literature, and obtained similar energies and oscillator strengths, thus confirming that the large differences between different calculations were mainly due to the different sets of configurations included and not to the use of different approximations and codes.

As our best "benchmark" configuration basis we have chosen the 48 configurations (48C) listed in Table 1 and used AUTOSTRUCTURE. The scaling parameters, λ_{nl}, for the potentials in which the orbital functions are calculated are given in Table 2. A positive scaling parameter indicates a statistical model potential while a negative scaling parameter signifies a correlation orbital that is calculated in a Coulomb potential with central charge number $Z|\lambda_{nl}|$ where $Z = 26$. The scaling parameters were chosen to minimise the equally weighted sum of the energies of the 24 lowest LS terms. Table 3 clearly shows good agreement between the energies $E_{\rm bench}$ and our experimental energies $E_{\rm exp}$ (Del Zanna 2010), in particular in terms of relative differences between levels.

In order to further improve the energies (and help the identification process), we have also applied term energy corrections (TEC) based on the observed energies of Del Zanna (2010)

Table 2. The target electron configuration basis (13C) and orbital scaling parameters.

Configurations		Scaling parameters[†]	
even	odd		
$3s^2\ 3p^4$	$3s\ 3p^5$	1s	1.4177
$3p^6$		2s	1.1233
$3s\ 3p^4\ 3d$	$3s^2\ 3p^3\ 3d$	2p	1.0655
	$3p^5\ 3d$	3s	1.1585
$3s^2\ 3p^2\ 3d^2$	$3s\ 3p^3\ 3d^2$	3p	1.1295
	$3s^2\ 3p\ 3d^3$	3d	1.1539
	$3s^2\ 3p^3\ 4s$	4s	1.1827
	$3s^2\ 3p^3\ 4d$	4d	1.1332
	$3s^2\ 3p^2\ 3d\ 4p$	4p	1.1593
	$3s^2\ 3p^2\ 3d\ 4f$	4f	1.2877

Notes. [(†)] See text for the physical significance of the scaling parameters.

(48CT). The TEC procedure (see, e.g. Zeippen et al. 1977; Nussbaumer & Storey 1978) introduces empirical corrections to the *LS* Hamiltonian matrix. The energies $E_{\rm bench}$ (TEC) are also shown in Table 3.

We then searched for a more limited set of configurations which provided energies (and weighted oscillator strengths gf) as close as possible to our 48CT calculation. We identified the basis of 13 configurations (13C) listed in Table 2. This was used as the target basis for our scattering calculation. The energies $E_{\rm target}$ from our target calculation (13C) agree well with those from the benchmark calculation and our experimental energies $E_{\rm exp}$ (Del Zanna 2010), as shown in Table 3. Recently, Ishikawa & Vilkas (2008) have published theoretical level energies for ions along the S I-like sequence obtained with the relativistic multireference many-body perturbation theory (hereafter referred to as MR-MP). This procedure yields very accurate energies, as known from previous work (see Ishikawa & Vilkas 2001; Del Zanna & Mason 2005, for Fe XII; Del Zanna & Ishikawa 2009, for Fe XVII; Ishikawa et al. 2009, for ions along the Ne I-like sequence). Table 3 clearly shows good agreement between our experimental energies $E_{\rm exp}$ (Del Zanna 2010) and those calculated by the MR-MP method. This confirms the reliability of our experimental energies (which were obtained independently before the MR-MP ones were published).

Table 4 lists the weighted oscillator strengths (gf) for a few of the most important transitions from the five levels of the ground configuration obtained from our benchmark basis (with and without TEC) and from the target basis. A remarkably good agreement between the gf values obtained with our target and benchmark calculations can be seen. Table 4 also lists gf values calculated by DT98, AK03, BDE02. Large differences are found for all the transitions from highly mixed levels. This includes for example the strong $^3P_2$–$^3P^o_2$ (1–38) transition for which AK03 calculated a gf of 3.4 and BDE02 of 4.0 compared to our best value of 2.5. The special case of the three highly mixed $J = 1$ levels is discussed in detail in the following Section. Note that the gf values obtained by F86 are often more accurate than any of the previous ab-initio calculations, because experimental adjustments were applied.

The large differences in gf values are directly reflected in large differences in collision strengths as we shall discuss later. This occurs because the main contribution for strong dipole-allowed transitions comes from high partial waves, where the collision strength is approximately proportional to the gf value for the transition.

Given that gf values from our target calculation are very similar to those of the benchmark + TEC one, it follows that transition probabilities are also very similar. Mixing and level ordering changes with any experimental adjustement, so transition probabilities to be associated with the present scattering calculation were calculated from the target calculation, by only adding all spin-spin interactions within the lowest four configurations, and by replacing energies with the experimental ones of Del Zanna (2010), whenever available.

2.3. Identification of the three $3s^2\ 3p^3\ 3d$ $J = 1$ levels

The strength of the interaction between levels of the same J and parity depends, to a first approximation, on the inverse of the energy difference between them. There are three $J = 1$ levels (indices 37, 39, 41 in Table 3) within the $3s^2\ 3p^3\ 3d$ which lie very close in energy, and hence interact strongly. This makes the definition of a good target, which represents these levels well, challenging. Another complexity lies in the fact that levels change their percentage composition and energy ordering along the isoelectronic sequence, as shown in Fig. 2. These results were obtained with AUTOSTRUCTURE applying the same benchmark basis (with correlation orbitals) and minimization procedure to all the ions in the sequence.

Whilst the lower and upper $J = 1$ levels are so strongly interacting that no designation in *LS* terms is meaningful, the middle $J = 1$ $3s^2\ 3p^3\ (^2D)\ 3d\ ^3S^o_1$ level remains identifiable throughout the sequence and becomes the "middle" $J = 1$ level for Fe XI.

The "labelling" used for these levels varies in the literature, however we prefer to call them "lower, middle and upper $J = 1$ level" here, the ordering being their energy relative to the ground state (our levels 37, 39 and 41 respectively).

To establish the identifications and energies of the mixed $J = 1$ levels we started by confirming the identification of the $3s^2\ 3p^3\ (^2D)\ 3d\ ^3P^o_2$ level (38 in Table 3). This level produces two strong decays to the ground $^3P^e_{2,1}$ levels (1–38 and 2–38). The 1–38 line is observed at 188.216 Å and is the second strongest Fe XI line in low-density plasmas. The 2–38 transition is observed at 192.813 Å, in exact agreement with the splitting between the ground $^3P^e_{2,1}$ levels, known from the strong forbidden line at 7891.8 Å.

The separation between the $^3P^o_{2,1}$ levels calculated in the 48C basis suggests an energy for the upper $J = 1$ level in broad agreement with the value 541 410 cm^{-3} derived by Bromage et al. (1977) and based on the following correct assignments made by those authors: 2–41: 189.129 Å; 3–41: 189.735 Å; 4–41: 198.549 Å. Jupén et al. (1993) labelled this level $^1P^o_1$ and incorrectly identified the 2–41 and 4–41 transitions with the lines observed at 192.619 and 202.405 Å in the laboratory spectra. BD96 had the same correct assignment as Bromage et al. (1977).

The middle $J = 1$ level $3s^2\ 3p^3\ (^2D)\ 3d\ ^3S^o_1$ (39) produces four observable transitions: 4–39, 1–39, 2–39, 3–39, correctly identified by Bromage et al. (1977) with the lines observed at 201.737, 187.446, 192.020 and 192.641 Å. Jupén et al. (1993) instead incorrectly identified the 1–39 transition with the line observed in the laboratory spectra at 184.704 Å. Note that the labelling for this level given by Jupén et al. (1993) was $^3P^o_1$. BD96 had the same correct assignment as Bromage et al. (1977). Keenan et al. (2005) incorrectly identified the 2–39, 3–39 transitions with the lines observed at 189.19 and 189.72 Å respectively.

Table 3. List of energies (cm^{-1}) for the lowest 48 levels of Fe XI.

i	Conf.	Lev.	E_{exp}	E_{target}	E_{bench}	E_{bench} (TEC)	E_{MR-MP}	E_{NIST}
1	$3s^2\ 3p^4$	$^3P^e_2$	0	0	0	0	0	0
2	$3s^2\ 3p^4$	$^3P^e_1$	12 667	12 587 (80)	12 371 (297)	12 397 (271)	12 667 (0)	12 667 (0)
3	$3s^2\ 3p^4$	$^3P^e_0$	14 306	14 245 (61)	14 283 (23)	14 155 (151)	14 312 (–6)	14 312 (–6)
4	$3s^2\ 3p^4$	$^1D^e_2$	37 743	39 504 (–1761)	38 324 (–581)	37 748 (–5)	37 743 (–1)	37 743 (–1)
5	$3s^2\ 3p^4$	$^1S^e_0$	80 831	80 190 (641)	83 640 (–2809)	80 842 (–11)	80 814 (16)	80 814 (16)
6	$3s\ 3p^5$	$^3P^o_2$	283 551	279 487 (4064)	283 764 (–213)	283 658 (–107)	283 739 (–188)	283 558 (–7)
7	$3s\ 3p^5$	$^3P^o_1$	293 158	289 178 (3980)	293 229 (–71)	293 089 (69)	293 315 (–157)	293 158 (0)
8	$3s\ 3p^5$	$^3P^o_0$	299 163	295 116 (4047)	299 059 (104)	298 953 (210)	299 308 (–145)	299 163 (0)
9	$3s\ 3p^5$	$^1P^o_1$	361 846	362 521 (–675)	365 012 (–3166)	361 678 (168)	361 675 (171)	361 842 (4)
10	$3s^2\ 3p^3\ 3d$	$^5D^o_0$	387 544	386 037 (1507)	389 671 (–2127)	387 427 (117)	387 622 (–78)	–
11	$3s^2\ 3p^3\ 3d$	$^5D^o_1$	387 726	386 278 (1448)	389 870 (–2144)	387 628 (98)	387 811 (–85)	–
12	$3s^2\ 3p^3\ 3d$	$^5D^o_2$	387 940	386 584 (1356)	390 118 (–2178)	387 866 (74)	388 020 (–80)	–
13	$3s^2\ 3p^3\ 3d$	$^5D^o_3$	388 268	387 049 (1219)	390 506 (–2238)	388 236 (32)	388 335 (–67)	–
14	$3s^2\ 3p^3\ 3d$	$^5D^o_4$	389 227	388 180 (1047)	391 510 (–2283)	389 244 (–17)	389 274 (–47)	–
15	$3s^2\ 3p^3\ 3d$	$^3D^o_2$	412 856	413 327 (–471)	416 494 (–3638)	413 082 (–226)	412 968 (–112)	–
16	$3s^2\ 3p^3\ 3d$	$^3D^o_3$	415 426	415 958 (–532)	418 774 (–3348)	415 618 (–192)	415 477 (–51)	–
17	$3s^2\ 3p^3\ 3d$	$^3D^o_1$	417 049	417 529 (–480)	420 300 (–3251)	417 205 (–156)	417 139 (–90)	–
18	$3s^2\ 3p^3\ 3d$	$^3F^o_2$	422 844	423 871 (–1027)	426 701 (–3857)	422 557 (287)	422 920 (–76)	–
19	$3s^2\ 3p^3\ 3d$	$^1S^o_0$	–	426 304	428 625	425 466	425 465	–
20	$3s^2\ 3p^3\ 3d$	$^3F^o_3$	426 022	427 435 (–1413)	429 980 (–3958)	425 712 (310)	426 149 (–127)	–
21	$3s^2\ 3p^3\ 3d$	$^3F^o_4$	430 522	432 267 (–1745)	434 444 (–3922)	430 102 (420)	430 589 (–67)	–
22	$3s^2\ 3p^3\ 3d$	$^3G^o_3$	–	452 321	453 512	448 623	448 615	–
23	$3s^2\ 3p^3\ 3d$	$^3G^o_4$	450 211	454 113 (–3902)	455 092 (–4881)	450 218 (–7)	450 228 (–17)	–
24	$3s^2\ 3p^3\ 3d$	$^3G^o_5$	452 416	456 642 (–4226)	457 218 (–4802)	452 414 (2)	452 413 (3)	–
25	$3s^2\ 3p^3\ 3d$	$^1G^o_4$	459 218	463 779 (–4561)	464 621 (–5403)	459 220 (–2)	459 231 (–13)	–
26	$3s^2\ 3p^3\ 3d$	$^1D^o_2$	–	468 495	472 489	466 545	466 458	–
27	$3s^2\ 3p^3\ 3d$	$^3D^o_1$	–	484 112	488 110	481 678	481 722	–
28	$3s^2\ 3p^3\ 3d$	$^3P^o_0$	–	484 177	488 573	482 071	482 618	–
29	$3s^2\ 3p^3\ 3d$	$^3P^o_1$	484 830	486 900 (–2070)	491 259 (–6429)	484 676 (154)	484 990 (–160)	–
30	$3s^2\ 3p^3\ 3d$	$^3F^o_3$	485 039	488 474 (–3435)	491 500 (–6461)	485 125 (–86)	485 081 (–42)	–
31	$3s^2\ 3p^3\ 3d$	$^3F^o_2$	–	489 360	492 645	486 234	486 227	–
32	$3s^2\ 3p^3\ 3d$	$^3F^o_4$	486 413	490 069 (–3656)	492 671 (–6258)	486 445 (–32)	486 412 (1)	–
33	$3s^2\ 3p^3\ 3d$	$^3D^o_2$	489 378	492 380 (–3002)	495 788 (–6410)	489 376 (2)	489 528 (–150)	–
34	$3s^2\ 3p^3\ 3d$	$^3P^o_2$	494 013	496 544 (–2531)	500 566 (–6553)	494 055 (–42)	494 053 (–40)	496 090 (–2077)
35	$3s^2\ 3p^3\ 3d$	$^3D^o_3$	497 235	500 555 (–3320)	503 664 (–6429)	497 216 (19)	497 452 (–217)	–
36	$3s^2\ 3p^3\ 3d$	$^1F^o_3$	525 260	530 347 (–5087)	532 842 (–7582)	525 278 (–18)	525 332 (–72)	–
37	$3s^2\ 3p^3\ 3d$	$^3P^{o\dagger}_1$	531 070	536 811 (–5741)	540 265 (–9195)	530 770 (300)	531 839 (–769)	526 480 (4590)
38	$3s^2\ 3p^3\ 3d$	$^3P^o_2$	531 304	537 000 (–5696)	541 300 (–9996)	531 551 (–247)	531 502 (–198)	531 290 (14)
39	$3s^2\ 3p^3\ 3d$	$^3S^{o\dagger}_1$	533 445	540 191 (–6746)	543 921 (–10 476)	533 838 (–393)	533 343 (102)	533 450 (–5)
40	$3s^2\ 3p^3\ 3d$	$^3P^o_0$	541 777	547 599 (–5822)	551 873 (–10 096)	542 143 (–366)	541 892 (–115)	541 720 (57)
41	$3s^2\ 3p^3\ 3d$	$^3P^{o\dagger}_1$	541 424	547 732 (–6308)	551 800 (–10 376)	541 729 (–305)	541 178 (246)	541 390 (34)
42	$3s^2\ 3p^3\ 3d$	$^3D^o_3$	554 321	561 699 (–7378)	564 972 (–10 651)	554 308 (13)	554 305 (16)	554 300 (21)
43	$3s^2\ 3p^3\ 3d$	$^3D^o_2$	561 615	569 308 (–7693)	572 350 (–10 735)	561 671 (–56)	561 556 (59)	561 610 (5)
44	$3s^2\ 3p^3\ 3d$	$^3D^o_1$	566 396	573 992 (–7596)	577 055 (–10 659)	566 321 (75)	566 299 (97)	566 380 (16)
45	$3s^2\ 3p^3\ 3d$	$^1D^o_2$	578 890	587 776 (–8886)	589 847 (–10 957)	578 887 (3)	578 539 (351)	578 860 (30)
46	$3s^2\ 3p^3\ 3d$	$^1F^o_3$	594 047	603 720 (–9673)	605 953 (–11 906)	594 047 (0)	594 518 (–471)	594 030 (17)
47	$3s^2\ 3p^3\ 3d$	$^1P^o_1$	623 101	631 099 (–7998)	636 559 (–13 458)	623 094 (7)	623 252 (–151)	623 080 (21)
48	$3p^6$	$^1S^e_0$	–	638 441	625 608	614 643	–	–

Notes. $^{(\dagger)}$ Lower, middle and upper $J = 1$.
The experimental level energies E_{exp} (Del Zanna 2010) are shown, together with those obtained from our scattering target E_{target}, those from our benchmark E_{bench}, those from our benchmark including TEC E_{bench}(TEC). We also list the values from the NIST compilation (E_{NIST}) and those calculated with the many-body perturbation theory (E_{MR-MP}) by Ishikawa & Vilkas (2008). Values in parentheses indicate differences with E_{exp}.

The lowest $J = 1$ level (level 37) is the most complex one, since the oscillator strength for its decay to the ground state is very sensitive to mixing. The gf values obtained in the benchmark, 48CT, calculation suggest that this transition should be third strongest from this ion. We identify this transition (1–37) with the strong 188.299 Å line. This line is very close to the 1–38 transition (188.216 Å), and is about 70% its intensity. The ratio in gf values means that (neglecting cascading) we predict a relative intensity of 60%, not too far from the measured value.

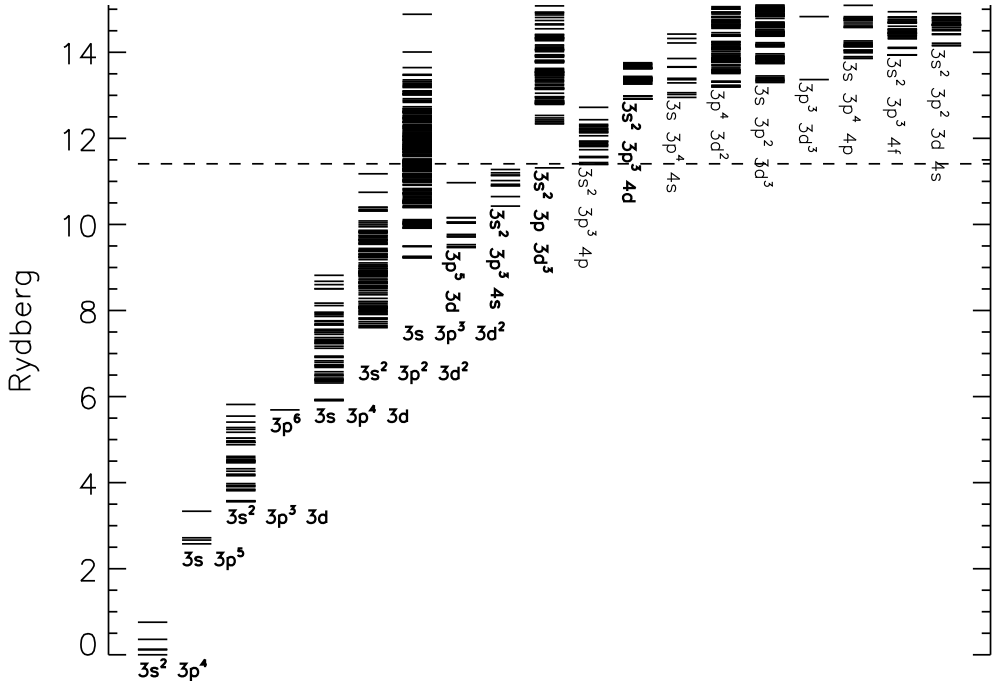

Fig. 1. The energetically lowest electron configurations of Fe XI. The energies are those of the benchmark calculation (48C), with all orbitals treated as spectroscopic. Configurations included within the target basis are highlighted in bold. Notice that the last two of the 13 target configurations are not shown in the plot, because they lie at higher energies, mixed with many other configurations. The $3s^2\ 3p^2\ 3d\ 4p$ levels start at 15.14 Ryd, while those of the $3s^2\ 3p^2\ 3d\ 4f$ configuration at 17.57 Ryd. The 145 terms which produce levels having energies below the dashed line have been retained for the scattering calculation.

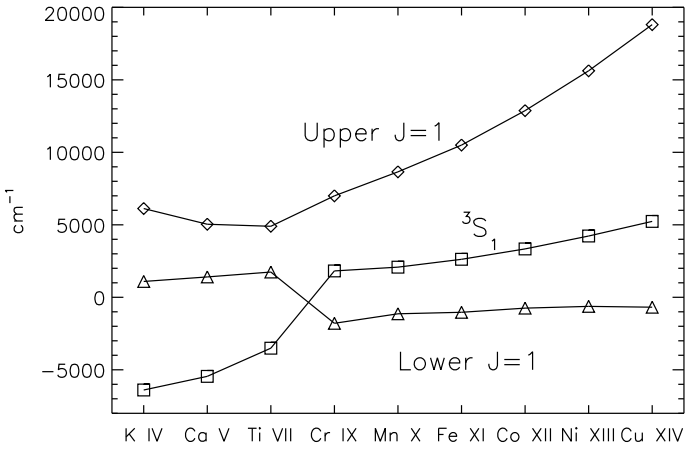

Fig. 2. Difference between the theoretical energies of the three $3s^2\ 3p^3\ 3d\ J = 1$ levels and the theoretical energy of the $3s^2\ 3p^3\ (^2D)\ 3d\ ^3P^o_2$ (level 38 in Table 3) along the S I-like sequence. The energies were calculated with SUPERSTRUCTURE and the same 48 configuration basis (our benchmark calculation, 48C).

Notice that AK03 and DT98 predict about 20% and 50% respectively.

Bromage et al. (1977) had a calculated wavelength for the 1–37 transition of 188.40 Å, very close to the actual value (188.299 Å), however they identified it with a weaker line observed at 189.940 Å. This error was caused by the fact that the 188.299 Å line was incorrectly assigned to an Fe XII transition. BD96 also gave the same incorrect assignment. Jupén et al. (1993) correctly identified this level, although they gave it an incorrect labelling ($^3S^o_1$) which has caused confusion in the literature.

As we have already seen, Ishikawa & Vilkas (2008) provided very good level energies, however in terms of identifications there are a few incorrect assignments, which originated from previous literature (Ishikawa, priv. comm.). Furthermore, the comparisons listed in Ishikawa & Vilkas (2008) between their results and those of Jupén et al. (1993) were not appropriate because the assignments followed the labelling of the levels given by Jupén et al. (1993), rather than their order in energy.

In terms of labelling, the National Institute of Standards and Technology (NIST) version 3 database[1] provides incorrect assignments for the three $J = 1$ levels. However, in terms of wavelength assignments, it provides correct identification for the middle and upper $J = 1$ levels, because the original assignments of Bromage et al. (1977) were adopted.

3. The scattering calculation

The R-matrix method used in the scattering calculation is described in Hummer et al. (1993) and Berrington et al. (1995). We performed the calculation in the inner region in *LS* coupling and included mass and Darwin relativistic energy shifts. The configuration basis describing the target for the present calculation is shown in Table 2 and Fig. 1. We used the AUTOSTRUCTURE code (Badnell 1997) to obtain the target radial wavefunctions using radial scaling parameters to minimize the equally-weighted sum of all LS term energies as listed in Table 2. The energies of the target terms are listed in Table 5, together with the experimental ones (Del Zanna 2010), which were used within the calculation to accurately position the resonance thresholds.

The set of 13 electron configurations gives rise to 465 *LS* terms and 1103 fine-structure levels. For the scattering calculation we have retained only the lowest 145 *LS* terms, which give

[1] http://physics.nist.gov

Table 4. Weighted absorption oscillator strengths (gf).

Upper level	Lower level				
u	$^3P_2^e$	$^3P_1^e$	$^3P_0^e$	$^1D_2^e$	$^1S_0^e$
34–$^3P_2^o$	202.42	207.75	–	219.17	–
48CT	0.13	3.3×10^{-2}	–	5.5×10^{-3}	–
48C	0.13	3.2×10^{-2}	–	5.2×10^{-3}	–
13C	0.16	3.6×10^{-2}	–	7.6×10^{-3}	–
DT98	7.4×10^{-2}	1.2×10^{-2}	–	5.8×10^{-3}	–
AK03	0.10	2.9×10^{-2}	–	2.7×10^{-3}	–
BDE02	0.11	3.1×10^{-2}	–	3.5×10^{-3}	–
F86	0.11	2.9×10^{-2}	–	–	–
35–$^3D_3^o$	201.12	–	–	217.64	–
48CT	2.2×10^{-2}	–	–	3.3×10^{-3}	–
48C	2.2×10^{-2}	–	–	3.1×10^{-3}	–
13C	2.1×10^{-2}	–	–	2.5×10^{-3}	–
DT98	5.0×10^{-2}	–	–	8.8×10^{-3}	–
AK03	1.9×10^{-2}	–	–	2.5×10^{-3}	–
BDE02	3.2×10^{-2}	–	–	2.9×10^{-3}	–
F86	5.0×10^{-2}	–	–	–	–
36–$^1F_3^o$	190.38	–	–	205.12	–
48CT	3.2×10^{-2}	–	–	3.6×10^{-4}	–
48C	2.7×10^{-2}	–	–	4.1×10^{-4}	–
13C	3.3×10^{-2}	–	–	2.1×10^{-3}	–
DT98	3.1×10^{-4}	–	–	2.2×10^{-2}	–
AK03	2.2×10^{-2}	–	–	7.4×10^{-4}	–
BDE02	1.7×10^{-2}	–	–	5.1×10^{-4}	–
F86	1.4×10^{-2}	–	–	–	–
37–$^3P_1^o$	188.30	192.90	193.51	202.71	222.10
48CT	1.5	2.5×10^{-3}	2.5×10^{-2}	0.18	2.1×10^{-2}
48C	1.6	3.7×10^{-2}	2.7×10^{-3}	4.2×10^{-2}	1.0×10^{-2}
13C	1.5	2.9×10^{-3}	6.5×10^{-2}	0.26	3.0×10^{-2}
DT98	1.3	0.20	2.7×10^{-2}	7.9×10^{-3}	1.5×10^{-2}
AK03	0.76	0.27	7.6×10^{-2}	2.6×10^{-2}	1.5×10^{-3}
BDE02	1.1	0.38	0.11	2.5×10^{-2}	1.4×10^{-3}
F86	1.6	–	2.1×10^{-2}	0.35	4.1×10^{-2}
38–$^3P_2^o$	188.22	192.81	–	202.61	–
48CT	2.6	0.56	–	5.0×10^{-2}	–
48C	2.6	0.58	–	4.9×10^{-2}	–
13C	2.6	0.57	–	4.7×10^{-2}	–
DT98	2.7	0.61	–	4.5×10^{-2}	–
AK03	3.4	0.69	–	4.8×10^{-2}	–
BDE02	4.0	0.79	–	4.4×10^{-2}	–
F86	2.9	0.60	–	5.1×10^{-2}	–
39–$^3S_1^o$	187.45	192.01	192.62	201.72	220.92
48CT	4.1×10^{-2}	0.45	0.25	1.0	4.3×10^{-2}
48C	7.7×10^{-3}	0.50	0.33	1.0	4.7×10^{-2}
13C	0.13	0.47	0.26	0.90	4.2×10^{-2}
DT98	0.32	0.48	0.43	8.0×10^{-2}	3.6×10^{-2}
AK03	0.97	0.68	0.60	0.35	6.1×10^{-4}
BDE02	1.1	0.83	0.72	0.39	7.0×10^{-5}
F86	0.24	0.49	0.22	1.1	4.2×10^{-2}

Notes. Only transitions between the five levels of the ground configuration and the $3s^2 3p^3 3d$ levels are shown. For each upper level, we list the index and LSJ from Table 3, together with the wavelength of the transition in Å. We then list the gf vales from our benchmark calculation with TEC (48CT) and without TEC (48C), those from our target basis (13C), together with a selection of values from the literature. DT98: Deb & Tayal (1998); AK03: Aggarwal & Keenan (2003a,b); BDE02: Bhatia et al. (2002); F86: Fawcett (1986).

Table 4. continued.

u	$^3P_2^e$	$^3P_1^e$	$^3P_0^e$	$^1D_2^e$	$^1S_0^e$
40–$^3P_0^o$	–	189.00	–	–	–
48CT	–	0.69	–	–	–
48C	–	0.70	–	–	–
13C	–	0.70	–	–	–
DT98	–	0.71	–	–	–
AK03	–	0.87	–	–	–
BDE02	–	1.0	–	–	–
F86	–	0.75	–	–	–
41–$^3P_1^o$	184.70	189.12	189.71	198.54	217.11
48CT	0.12	0.59	0.52	0.69	7.7×10^{-2}
48C	0.12	0.52	0.47	0.85	8.6×10^{-2}
13C	8.6×10^{-2}	0.59	0.49	0.77	9.9×10^{-2}
DT98	0.12	0.36	0.35	0.11	0.10
AK03	2.8×10^{-2}	9.8×10^{-2}	0.24	2.2	9.5×10^{-2}
BDE02	3.7×10^{-2}	0.12	0.26	2.5	8.6×10^{-2}
F86	0.16	0.76	0.66	–	6.1×10^{-2}
42–$^3D_3^o$	180.40	–	–	193.58	–
48CT	4.6	–	–	2.8×10^{-3}	–
48C	4.7	–	–	3.4×10^{-3}	–
13C	4.8	–	–	2.6×10^{-3}	–
DT98	4.7	–	–	2.8×10^{-4}	–
AK03	5.3	–	–	3.9×10^{-3}	–
BDE02	6.2	–	–	5.2×10^{-3}	–
F86	5.3	–	–	–	–
43–$^3D_2^o$	178.06	182.16	–	190.88	–
48CT	0.65	2.6	–	8.3×10^{-2}	–
48C	0.67	2.6	–	8.1×10^{-2}	–
13C	0.68	2.6	–	7.8×10^{-2}	–
DT98	0.67	2.5	–	0.12	–
AK03	0.62	2.9	–	0.15	–
BDE02	0.72	3.4	–	0.18	–
F86	0.75	2.9	–	0.13	–
44–$^3D_1^o$	176.55	180.59	181.13	189.16	205.95
48CT	3.4×10^{-2}	0.81	1.1	6.0×10^{-3}	2.0×10^{-4}
48C	3.6×10^{-2}	0.82	1.2	6.1×10^{-3}	2.0×10^{-4}
13C	3.7×10^{-2}	0.83	1.2	4.0×10^{-3}	2.4×10^{-4}
DT98	3.8×10^{-2}	0.81	1.2	6.0×10^{-3}	3.5×10^{-4}
AK03	3.3×10^{-2}	0.91	1.3	6.9×10^{-2}	1.1×10^{-2}
BDE02	3.9×10^{-2}	1.1	1.5	5.5×10^{-2}	3.2×10^{-3}
F86	4.0×10^{-2}	0.92	1.3	–	–
45–$^1D_2^o$	172.74	176.61	–	184.79	–
48CT	4.8×10^{-4}	0.15	–	2.6	–
48C	5.0×10^{-4}	0.15	–	2.7	–
13C	5.0×10^{-4}	0.15	–	2.7	–
DT98	6.2×10^{-4}	0.19	–	2.6	–
AK03	1.5×10^{-2}	0.29	–	2.3	–
BDE02	1.3×10^{-2}	0.29	–	3.1	–
F86	–	0.20	–	3.3	–
46–$^1F_3^o$	168.34	–	–	179.76	–
48CT	8.2×10^{-3}	–	–	5.0	–
48C	9.2×10^{-3}	–	–	5.1	–
13C	7.5×10^{-3}	–	–	5.2	–
DT98	3.8×10^{-3}	–	–	5.1	–
AK03	1.9×10^{-2}	–	–	6.3	–
BDE02	1.7×10^{-2}	–	–	7.1	–
F86	–	–	–	5.6	–

rise to 365 levels and 66 430 transitions. The expansion of each scattered electron partial wave was done over a basis of 25 functions within the R-matrix boundary, and the partial wave expansion extended to a maximum total orbital angular momentum quantum number of $L = 16$.

The outer region calculation used the intermediate-coupling frame transformation method (ICFT) described by Griffin et al. (1998), in which the transformation to intermediate coupling

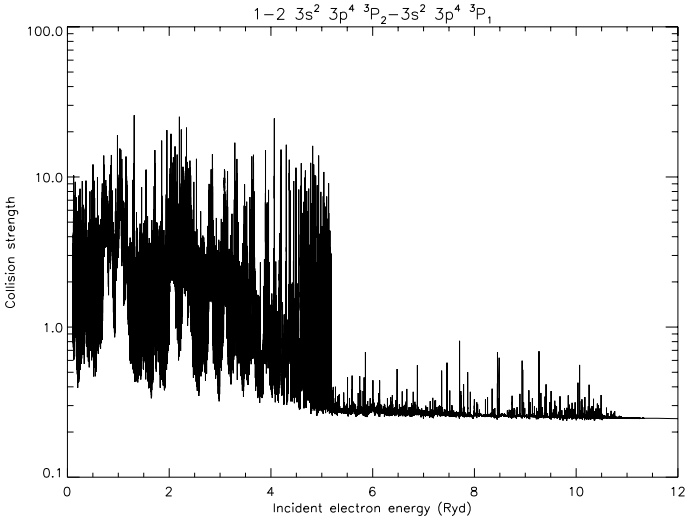

Fig. 3. Collision strength for the 1–2 transition.

Table 5. Theoretical energies of target terms $E_{\rm target}$ (Rydberg), with the experimental energies $E_{\rm exp}$ adopted for the scattering calculation. Only the terms from the lowest 4 configurations are shown here.

i	Conf.	Term	$E_{\rm target}$	$E_{\rm exp}$
1	$3s^2\ 3p^4$	^{3}P	0.000	0.000
2	$3s^2\ 3p^4$	^{1}D	0.281	0.344
3	$3s^2\ 3p^4$	^{1}S	0.631	0.737
4	$3s\ 3p^5$	^{3}P^o	2.531	2.629
5	$3s\ 3p^5$	^{1}P^o	3.234	3.296
6	$3s^2\ 3p^3\ 3d$	^{5}D^o	3.478	3.540
7	$3s^2\ 3p^3\ 3d$	^{3}D^o	3.738	3.781
8	$3s^2\ 3p^3\ 3d$	^{1}S^o	3.830	3.877
9	$3s^2\ 3p^3\ 3d$	^{3}F^o	3.843	3.892
10	$3s^2\ 3p^3\ 3d$	^{3}G^o	4.087	4.107
11	$3s^2\ 3p^3\ 3d$	^{1}G^o	4.182	4.185
12	$3s^2\ 3p^3\ 3d$	^{1}D^o	4.194	4.251
13	$3s^2\ 3p^3\ 3d$	^{3}F^o	4.372	4.429
14	$3s^2\ 3p^3\ 3d$	^{3}P^o	4.410	4.461
15	$3s^2\ 3p^3\ 3d$	^{3}D^o	4.439	4.481
16	$3s^2\ 3p^3\ 3d$	^{1}F^o	4.744	4.787
17	$3s^2\ 3p^3\ 3d$	^{3}S^o	4.850	4.850
18	$3s^2\ 3p^3\ 3d$	^{3}P^o	4.858	4.858
19	$3s^2\ 3p^3\ 3d$	^{1}P^o	4.866	4.861
20	$3s^2\ 3p^3\ 3d$	^{3}D^o	5.107	5.096
21	$3s^2\ 3p^3\ 3d$	^{1}D^o	5.275	5.275
22	$3s^2\ 3p^3\ 3d$	^{1}F^o	5.424	5.413
23	$3s^2\ 3p^3\ 3d$	^{1}P^o	5.665	5.678
24	$3p^6$	^{1}S	5.755	

uses the so-called term-coupling coefficients (TCCs), and is complete up to a total angular momentum quantum number, $J = 23/2$. We have supplemented this calculation, which includes exchange, with a non-exchange calculation that extends from $J = 25/2$ to $J = 73/2$. Dipole-allowed transitions were topped-up to infinite partial wave using an intermediate coupling version of the Coulomb-Bethe method as described by Burgess (1974) while non-dipole allowed transitions were topped-up assuming that the collision strengths form a geometric progression in J for $J > 73/2$ (see Badnell & Griffin 2001).

3.1. Collision strengths

The R-matrix calculation extended to an incident electron energy of 141 Ry. At higher energies we used the method of scaling and

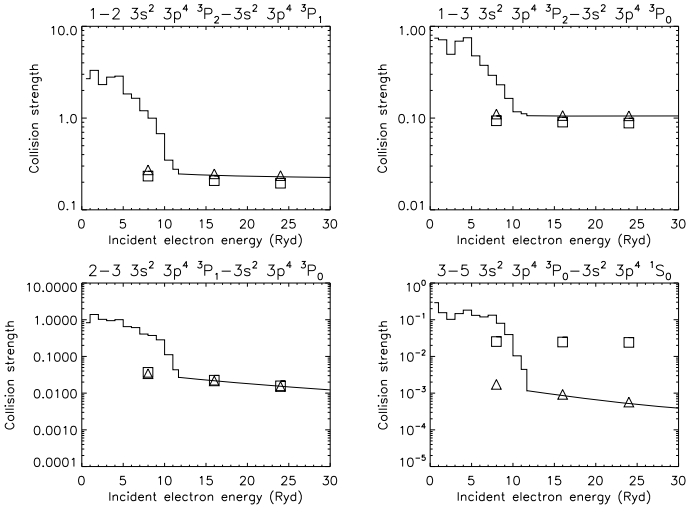

Fig. 4. Collision strengths for transitions within the ground configuration, averaged over 1 Ryd. Boxes indicate the GT99 values, while triangles the AK03 ones.

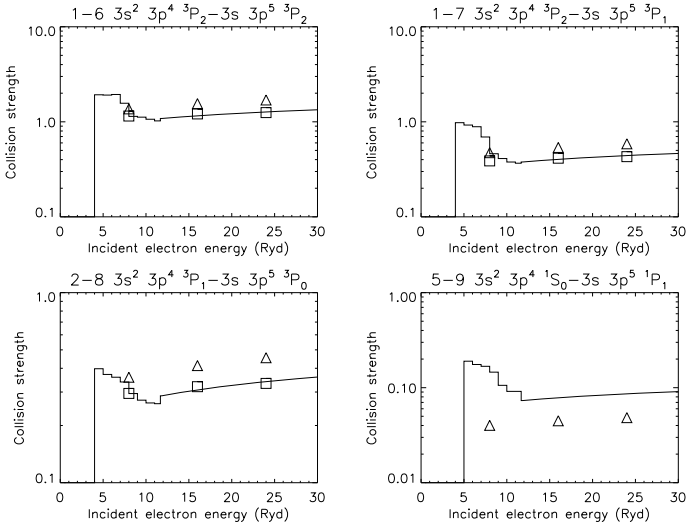

Fig. 5. Collision strengths for a selection of $3s^2\ 3p^4$–$3s\ 3p^5$ transitions, averaged over 1 Ryd. Boxes indicate the GT99 values, while triangles the AK03 ones.

extrapolating to the appropriate high-energy limits as described in Burgess & Tully (1992). The high-energy limits were calculated with AUTOSTRUCTURE for both optically-allowed (see Burgess et al. 1997) and forbidden transitions (see Chidichimo et al. 2003).

The collision strengths of all the transition from the levels of the ground configuration have been visually inspected, to check that the values converged to the respective high-energy limits.

Figure 3 shows as an example the collisions strengths of the 1–2 transition in the resonance region. Notice the large number of resonances. Figures 4–7 show a sample of collision strengths, averaged over 1 Ry for an easier comparison with literature data. At energies above all resonances, good agreement was found with the values calculated by GT99 and AK03 for transitions within the ground configuration (see Fig. 4), with the exception of the $^3P_0$–$^1S_0$ values calculated by GT99. Good agreement is found for the transitions to $3s\ 3p^5$ calculated by GT99 (see Fig. 5), with some differences with the AK03 values. Larger differences are found for transitions to the $3s^2\ 3p^3\ 3d$ levels (see Fig. 6). The large discrepancies seen in the gf values for the

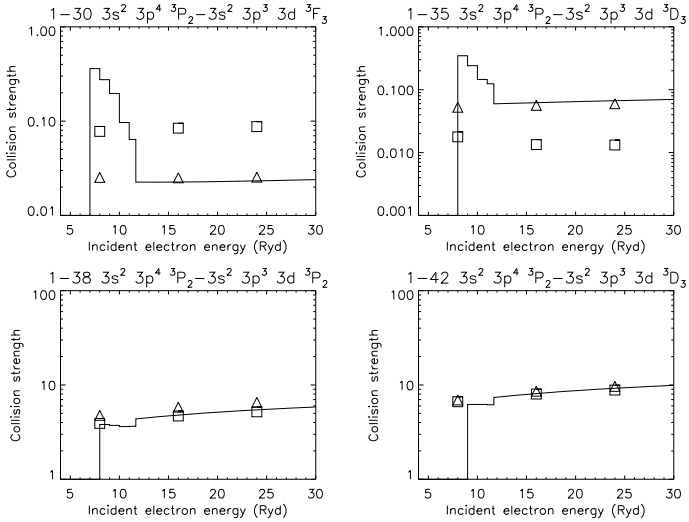

Fig. 6. Collision strengths for a selection of $3s^2\ 3p^4$–$3s^2\ 3p^3\ 3d$ transitions, averaged over 1 Ryd. Boxes indicate the GT99 values, while triangles the AK03 ones.

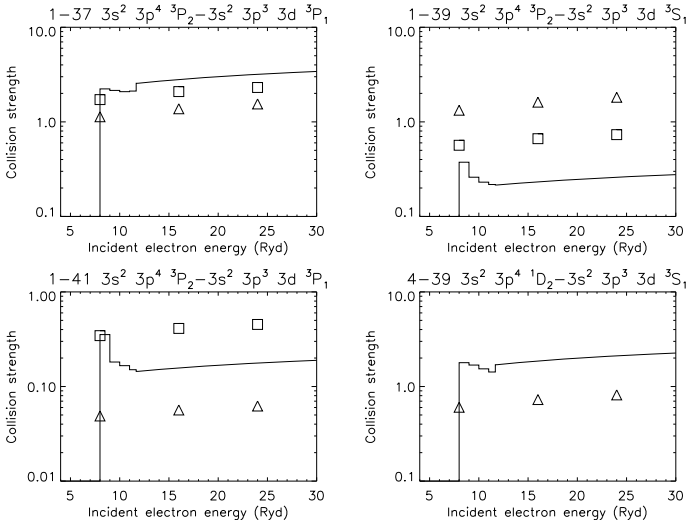

Fig. 7. Collision strengths for transitions involving the three $J = 1$ levels, averaged over 1 Ryd. Boxes indicate the GT99 values, while triangles the AK03 ones.

especially "troublesome" transitions to the $J = 1$ levels are reflected in the large discrepancies in the collision strengths seen in Fig. 7.

3.2. The effective collision strengths

We calculated the temperature-dependent effective collision strength $\Upsilon(i - j)$ by assuming a Maxwellian electron distribution:

$$\Upsilon(i-j) = \int_0^\infty \Omega(i-j)\exp(-E_j/kT)\,\mathrm{d}(E_j/kT)$$

where E_j is the final energy of the colliding electron (after excitation has occurred) and k is the Boltzmann constant. We performed the numerical integration by linearly interpolating the $\Omega(i - j)\exp(-E_j/kT)$ data points and extrapolating to the high-energy limit.

The effective collision strengths Υ were calculated in a wide temperature range ($1.\times10^4$–$1.\times10^8$ K) to cover all astrophysical applications. A selection of values for transitions from the ground state up to the $3p^6\ ^1S_0$ level (48) are shown in Table 6 (the full dataset is available on-line). Given that results obtained with the intermediate-coupling frame transformation are known to be comparable in accuracy to those obtained using a full Breit-Pauli R-matrix calculation, the main uncertainty in the rates derives from the accuracy of the target. Rates for most strong transitions are expected to have a relative accuracy of 10% or so, although those involved with the highly mixed levels 37, 39, 41 are expected to be less accurate. Comparison with experimental data (Del Zanna 2010) indicates agreement within 20% for most line intensities, which is encouraging.

Table 6. Effective collision strengths for a selection of transitions from the ground state, at 4 temperatures (log T[K] = 5.7, 6.0, 6.3, 6.7; $a^b = a \times 10^b$).

i–j	5.70	6.00	6.30	6.70
1–2	1.96	1.35	8.78^{-1}	5.10^{-1}
1–3	4.83^{-1}	3.47^{-1}	2.44^{-1}	1.66^{-1}
1–4	1.59	1.06	6.47^{-1}	3.27^{-1}
1–5	2.26^{-1}	1.43^{-1}	8.28^{-2}	3.74^{-2}
1–6	1.39	1.27	1.25	1.36
1–7	5.79^{-1}	4.95^{-1}	4.63^{-1}	4.83^{-1}
1–8	7.25^{-2}	4.31^{-2}	2.44^{-2}	1.10^{-2}
1–9	2.27^{-1}	1.55^{-1}	1.11^{-1}	8.04^{-2}
1–10	4.15^{-2}	2.56^{-2}	1.55^{-2}	7.64^{-3}
1–11	1.29^{-1}	8.12^{-2}	5.11^{-2}	2.87^{-2}
1–12	2.17^{-1}	1.38^{-1}	8.83^{-2}	5.08^{-2}
1–13	3.15^{-1}	1.99^{-1}	1.25^{-1}	6.67^{-2}
1–14	3.77^{-1}	2.42^{-1}	1.53^{-1}	7.99^{-2}
1–15	2.24^{-1}	1.50^{-1}	1.03^{-1}	6.83^{-2}
1–16	3.25^{-1}	2.09^{-1}	1.34^{-1}	7.66^{-2}
1–17	1.10^{-1}	6.99^{-2}	4.57^{-2}	2.96^{-2}
1–18	1.46^{-1}	8.83^{-2}	5.27^{-2}	2.72^{-2}
1–19	3.10^{-2}	2.07^{-2}	1.36^{-2}	7.36^{-3}
1–20	1.98^{-1}	1.24^{-1}	7.85^{-2}	4.67^{-2}
1–21	2.43^{-1}	1.56^{-1}	1.04^{-1}	6.81^{-2}
1–22	1.36^{-1}	8.55^{-2}	5.37^{-2}	3.07^{-2}
1–23	1.76^{-1}	1.13^{-1}	7.37^{-2}	4.51^{-2}
1–24	2.37^{-1}	1.67^{-1}	1.24^{-1}	9.64^{-2}
1–25	1.74^{-1}	1.11^{-1}	7.06^{-2}	3.82^{-2}
1–26	1.14^{-1}	7.68^{-2}	5.35^{-2}	3.66^{-2}
1–27	7.17^{-2}	5.47^{-2}	4.48^{-2}	4.01^{-2}
1–28	1.68^{-2}	1.04^{-2}	6.17^{-3}	2.96^{-3}
1–29	1.39^{-1}	1.27^{-1}	1.26^{-1}	1.40^{-1}
1–30	9.05^{-2}	6.14^{-2}	4.40^{-2}	3.39^{-2}
1–31	5.37^{-2}	3.30^{-2}	1.98^{-2}	1.03^{-2}
1–32	1.05^{-1}	6.51^{-2}	3.92^{-2}	1.97^{-2}
1–33	1.04^{-1}	8.00^{-2}	6.72^{-2}	6.31^{-2}
1–34	3.29^{-1}	3.23^{-1}	3.39^{-1}	3.95^{-1}
1–35	1.31^{-1}	1.02^{-1}	8.61^{-2}	8.06^{-2}
1–36	9.47^{-2}	8.32^{-2}	7.85^{-2}	8.26^{-2}
1–37	2.30	2.48	2.78	3.37
1–38	3.96	4.27	4.77	5.78
1–39	2.23^{-1}	2.25^{-1}	2.40^{-1}	2.80^{-1}
1–40	1.03^{-2}	7.07^{-3}	4.65^{-3}	2.56^{-3}
1–41	1.52^{-1}	1.53^{-1}	1.63^{-1}	1.91^{-1}
1–42	6.71	7.24	8.09	9.82
1–43	9.69^{-1}	1.04	1.15	1.38
1–44	7.47^{-2}	7.34^{-2}	7.58^{-2}	8.51^{-2}
1–45	3.26^{-2}	2.36^{-2}	1.65^{-2}	1.02^{-2}
1–46	5.34^{-2}	4.33^{-2}	3.54^{-2}	2.89^{-2}
1–47	1.17^{-2}	8.21^{-3}	5.42^{-3}	2.90^{-3}
1–48	4.60^{-3}	4.05^{-3}	3.81^{-3}	3.82^{-3}

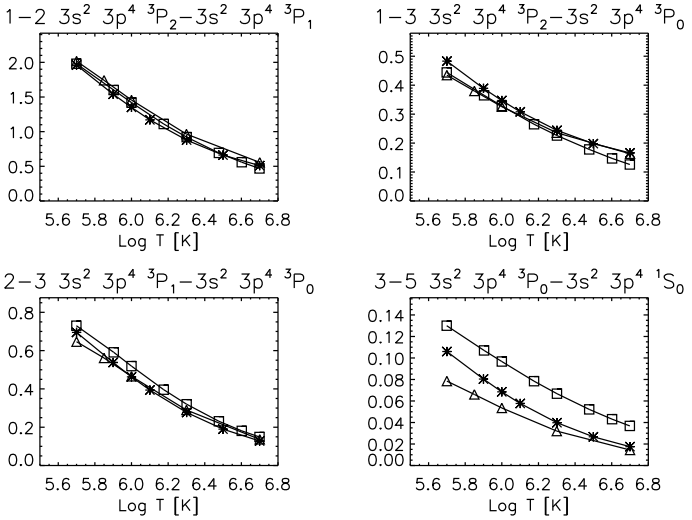

Fig. 8. Effective collision strengths for transitions within the ground configuration. Boxes indicate the GT99 values, while triangles the AK03 ones.

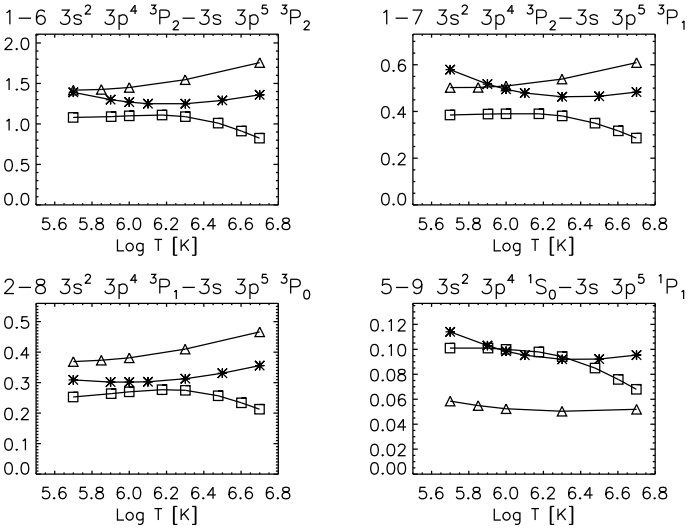

Fig. 9. Effective collision strengths for a selection of $3s^2\ 3p^4$–$3s\ 3p^5$ transitions. Boxes indicate the GT99 values, while triangles the AK03 ones.

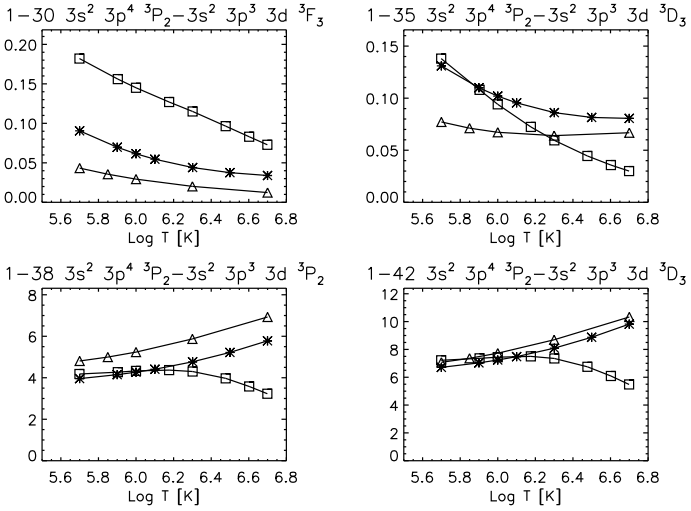

Fig. 10. Effective collision strengths for a selection of $3s^2\ 3p^4$–$3s^2\ 3p^3\ 3d$ transitions. Boxes indicate the GT99 values, while triangles the AK03 ones.

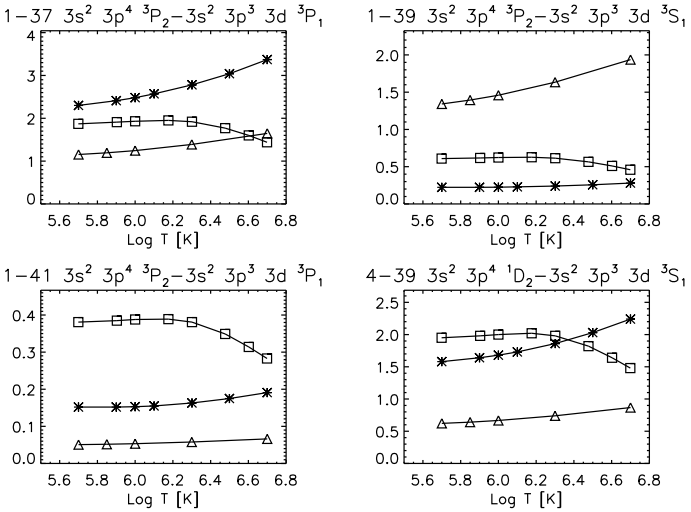

Fig. 11. Effective collision strengths for transitions involving the three $J = 1$ levels. Boxes indicate the GT99 values, while triangles the AK03 ones.

Figures 8–11 show effective collision strengths for the same selection of transitions for which we plotted collision strengths. In Fig. 12 we plot our effective collision strengths for dipole-allowed transitions at 10^6 K against the AK03 values. Strong transitions with differences of more than a factor of two are labelled. In Fig. 13 we plot our effective collision strengths for dipole-allowed transitions at two temperatures against the GT99 values. In Fig. 14 we plot our values for forbidden transitions at a low temperature, against the AK03 and GT99 values.

Significant differences with the R-matrix calculations of GT99 and AK03 are found for a large number of transitions. The largest (more than a factor of two) differences are, as expected from the large discrepancies seen in the gf values, for the "troublesome" transitions to the $J = 1$ levels (Figs. 11–13). We believe that most of the differences at 10^6 K are due to the different target basis.

At high temperatures, the AK03 values tend to have the correct behaviour overall, while the GT99 values for all the strong dipole-allowed transitions are underestimated as shown in Figs. 9–11, 13. This does not occur for the forbidden transitions (see Figs. 8, 14). The fact that good agreement in the collision strengths is found at low energies possibly means missing high partial wave and/or high energy contributions to the dipole-allowed collision strengths in the work of Gupta & Tayal (1999b). The same finding is reported in a study of Fe XIII by Storey & Zeippen (2009).

At low temperatures, and in particular for the forbidden transitions, very large differences are found, in particular with the AK03 values which are consistently lower, as Fig. 14 shows. The most likely explanation is the additional resonances present in our calculation due to the larger number of target states, which are particularly significant at lower temperatures.

3.3. Convergence on energy resolution

Several calculations of the collision strengths $\Omega(i-j)$ were made using different energy resolutions. A coarse mesh of 0.75 Ry was used beyond the resonance region of the exchange calculation and over the entire energy range of the non-exchange

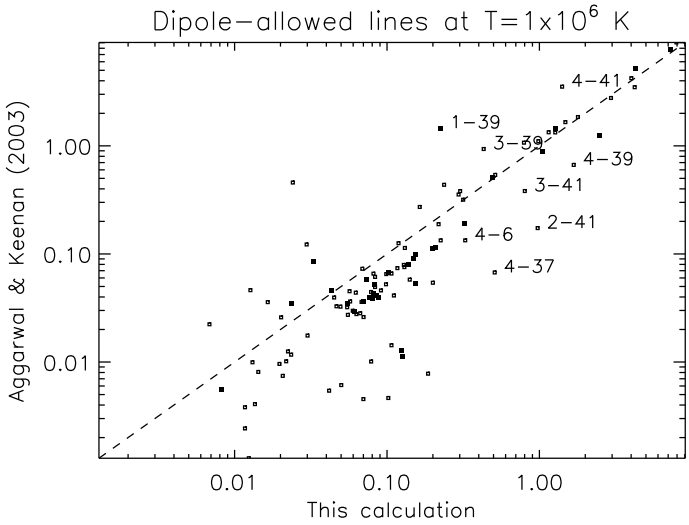

Fig. 12. Comparison of effective collision strengths for dipole-allowed transitions at $T = 10^6$ K, compared to AK03. Strong transitions with values differing by more than a factor of 2 are labelled with our level indices.

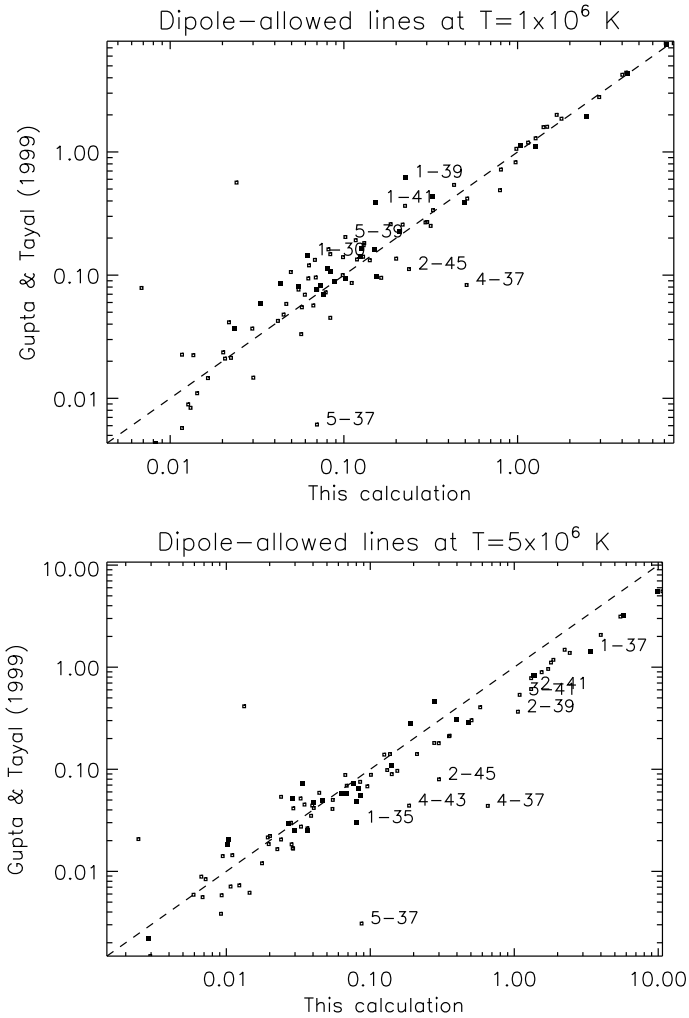

Fig. 13. Comparison of effective collision strength for dipole-allowed transitions at two temperatures, compared to GT99. Strong transitions with values differing by more than a factor of 2 are labelled with our level indices.

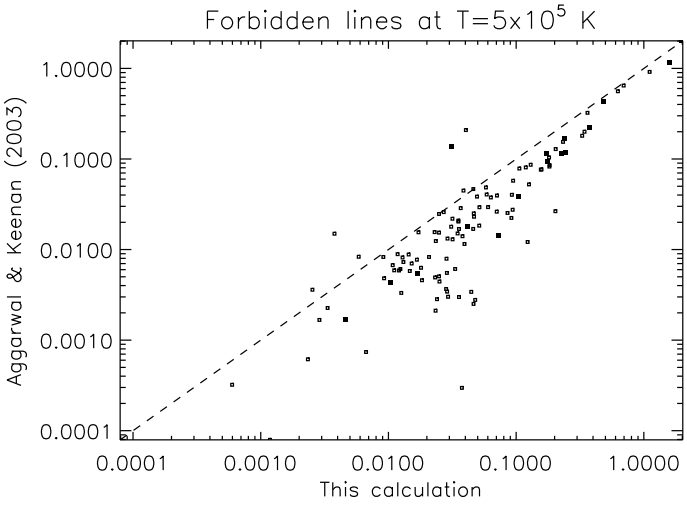

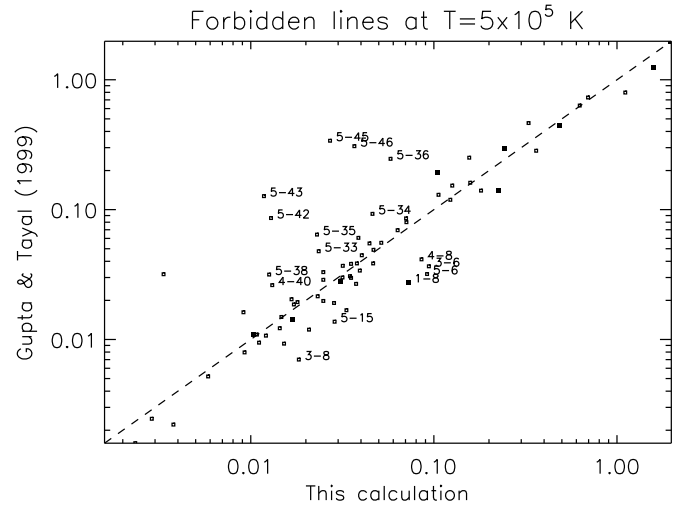

Fig. 14. Comparison of effective collision strength for forbidden transitions at 5×10^5 K. Transitions with values differing by more than a factor of 2 are labelled with our level indices.

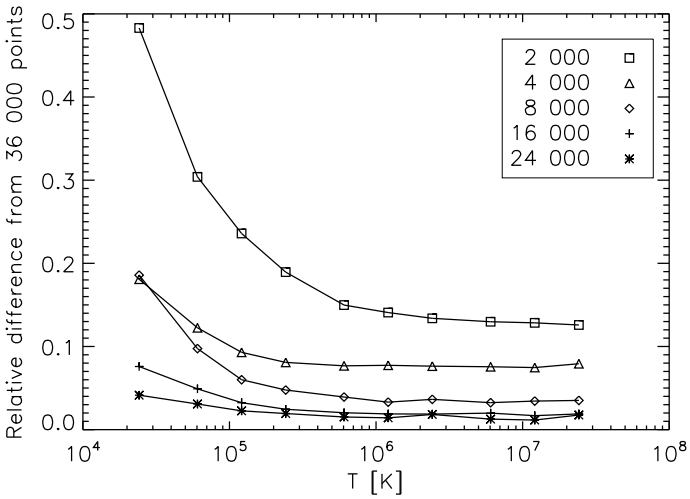

Fig. 15. Maximum relative difference between the thermally-averaged collision strengths calculated with 36 000 mesh points in the resonance region, and a number of increasing mesh points from 2000 to 24 000. Only transitions from the $3s^23p^4$ levels to $3s^23p^4$, $3s\ 3p^5$, $3s^23p^33d$ and $3p^6$ were considered.

calculation up to an energy of 141 Ry in all the calculations. In order to test the importance of the energy resolution in the resonance region, the number of energy points was increased from 2000 up to 32 000 in steps of 2000 points. For each of these cases, we calculated the final collision strength and the thermally-averaged ones. We have then considered all the transitions from the ground configuration to the other spectroscopically-important configurations shown in Table 3, and calculated the maximum deviation of the thermally-averaged collision strength for a set of temperatures. The results are shown in Fig. 15, where it is clear that for a number of mesh points larger than 16 000 the maximum deviation is less than 10% at all temperatures.

4. Summary and conclusions

A number of scattering calculations for electron collisional excitation of Fe XI have been produced in the literature, none of which have been able to correctly represent the excitation for some of the most important levels for the EUV spectrum of this ion.

After a long iterative procedure in which we combined experimental data with structure calculations along the S I-like sequence, we have been able to identify a good basis for our scattering calculations, and to provide reliable energies and oscillator strengths.

During this procedure we were able to identify most of the previously unknown fine-structure levels within the important $3s^2 3p^3 3d$ configuration, which gives rise to strong EUV transitions observed for example by Hinode/EIS.

In terms of collision strengths, we find large differences with values found in previous literature, in particular for those few transitions arising from levels highly mixed and very sensitive to the target. We believe that several outstanding discrepancies between astronomical observations and theory are resolved with this new calculation, as described in Del Zanna (2010).

Acknowledgements. G.D.Z. acknowledges support from STFC via the Advanced Fellowship program. We acknowledge support from STFC (UK) via the APAP network grant. We thank N. R. Badnell for various advices on the calculations. G.D.Z. warmly thanks B. C. Fawcett for continuous support and encouragement, together with many exchanges of correspondence.

References

Aggarwal, K. M., & Keenan, F. P. 2003a, A&A, 399, 799
Aggarwal, K. M., & Keenan, F. P. 2003b, MNRAS, 338, 412
Badnell, N. R. 1997, J. Phys. B Atomic Molecular Physics, 30, 1
Badnell, N. R., & Griffin, D. C. 2001, J. Phys. B Atomic Molecular Physics, 34, 681
Behring, W. E., Cohen, L., Doschek, G. A., & Feldman, U. 1976, ApJ, 203, 521
Berrington, K. A., Eissner, W. B., & Norrington, P. H. 1995, Comp. Phys. Comm., 92, 290
Bhatia, A. K., & Doschek, G. A. 1996, Atomic Data and Nuclear Data Tables, 64, 183
Bhatia, A. K., Doschek, G. A., & Eissner, W. 2002, Atomic Data and Nuclear Data Tables, 82, 211
Bromage, G. E., Cowan, R. D., & Fawcett, B. C. 1977, Phys. Scr, 15, 177
Burgess, A. 1974, J. Phys. B Atomic Molecular Physics, 7, L364
Burgess, A., Chidichimo, M. C., & Tully, J. A. 1997, J. Phys. B Atomic Molecular Physics, 30, 33
Burgess, A., & Tully, J. A. 1992, A&A, 254, 436
Chidichimo, M. C., Badnell, N. R., & Tully, J. A. 2003, A&A, 401, 1177
Deb, N. C., & Tayal, S. S. 1998, Atomic Data and Nuclear Data Tables, 69, 161
Del Zanna, G. 2010, A&A, 514, A41
Del Zanna, G., & Ishikawa, Y. 2009, A&A, 508, 1517
Del Zanna, G., & Mason, H. E. 2005, A&A, 433, 731
Eissner, W., Jones, M., & Nussbaumer, H. 1974, Computer Physics Communications, 8, 270
Fawcett, B. C. 1986, Atomic Data and Nuclear Data Tables, 35, 185
Fawcett, B. C., & Gabriel, A. H. 1965, ApJ, 141, 343
Fawcett, B. C., & Gabriel, A. H. 1966, Proc. Phys. Soc., 88, 262
Fritzsche, S., Dong, C. Z., & Träbert, E. 2000, MNRAS, 318, 263
Gabriel, A. H., Fawcett, B. C., & Jordan, C. 1965, Nature, 206, 390
Gabriel, A. H., Fawcett, B. C., & Jordan, C. 1966, Proc. Phys. Soc., 87, 825
Griffin, D. C., Badnell, N. R., & Pindzola, M. S. 1998, J. Phys. B Atomic Molecular Physics, 31, 3713
Gupta, G. P., & Tayal, S. S. 1999a, ApJ, 510, 1078
Gupta, G. P., & Tayal, S. S. 1999b, ApJS, 123, 295
Hummer, D. G., Berrington, K. A., Eissner, W., et al. 1993, A&A, 279, 298
Ishikawa, Y., & Vilkas, M. J. 2001, Phys. Rev. A, 63, 042506
Ishikawa, Y., & Vilkas, M. J. 2008, Phys. Rev. A, 78, 042501
Ishikawa, Y., López-Encarnación, J. M., & Träbert, E. 2009, Phys. Scr., 79, 025301
Jupén, C., Isler, R. C., & Trabert, E. 1993, MNRAS, 264, 627
Keenan, F. P., Aggarwal, K. M., Ryans, R. S. I., et al. 2005, ApJ, 624, 428
Mason, H. E. 1975, MNRAS, 170, 651
Mason, H. E., & Nussbaumer, H. 1977, A&A, 54, 547
Mendoza, C., & Zeippen, C. J. 1983, MNRAS, 202, 981
Nussbaumer, H., & Storey, P. J. 1978, A&A, 64, 139
Storey, P. J., & Zeippen, C. 2010, A&A, 511, A78
Träbert, E., Calamai, A. G., Gwinner, G., et al. 2003, J. Phys. B Atomic Molecular Physics, 36, 1129
Young, P. R., Del Zanna, G., Mason, H. E., et al. 2007, PASJ, 59, 857
Zeippen, C. J., Seaton, M. J., & Morton, D. C. 1977, MNRAS, 181, 527